https://doi.org/10.48048/tis.2024.7200

# Synthesis of Flower-Like $CuBi_2O_4$ Microspheres and Its Photocatalytic Activity

**Rapeepat Muankaew[1], Chompunut Banphot[1], Punyanuch Thammaacheep[1], Panatda Jannoey[2], Wilawan Khanitchaidecha[3], Auppatham Nakaruk[3] and Duangdao Channei[1,4,*]**

*[1]Department of Chemistry, Faculty of Science, Naresuan University, Phitsanulok 65000, Thailand*
*[2]Department of Biochemistry, Faculty of Medical Science, Naresuan University, Phitsanulok 65000, Thailand*
*[3]Centre of Excellence for Innovation and Technology for Water Treatment, Faculty of Engineering, Naresuan University, Phitsanulok 65000, Thailand*
*[4]Center of Excellence in Petroleum, Petrochemicals and Advanced Materials, Faculty of Science, Naresuan University, Phitsanulok 65000, Thailand*

**([*]Corresponding author's e-mail: duangdaoc.nu.ac.th)**

*Received: 11 June 2023, Revised: 22 August 2023, Accepted: 29 August 2023, Published: 1 January 2024*

**Abstract**

In this study, visible-light copper bismuth oxide ($CuBi_2O_4$) photocatalyst were synthesized via co-precipitation ($CuBi_2O_4$-C) and microwave-assisted methods ($CuBi_2O_4$-M). The X-ray powder diffraction (XRD) analysis reveals the presence of pure tetragonal, along with band gaps of 2.9 eV in both samples. The microwave-assisted method produced flower-like $CuBi_2O_4$ microspheres, which had a larger BET surface area and demonstrated the highest photocatalytic performance, approximately 83.4 % in the decolorization of malachite green (MG) dye under visible light. Therefore, the research suggested a facile strategy for the fast synthesis of $CuBi_2O_4$ microspheres under mild reaction conditions. The use of microwave heat treatment is a faster and more efficient way to photocatalyst materials, while also being cost-effective and energy-saving.

**Keywords:** Copper bismuth oxide, Microwave-assisted method, Photocatalysis, Malachite green

## Introduction

Malachite green (MG) is a type of dye from the triphenylmethane family that has been extensively utilized in various industries including ceramics, leather, textile, food coloring, and cell coloring. It has also been employed in the aquaculture industry to disinfect and heal scratches on fish as well as protect against bacterial infections due to its effectiveness. Unfortunately, researchers discovered in the 1990s that malachite green and its reduced forms are extremely toxic, persistent, carcinogenic, and mutagenic [1].

If released into water bodies, it could cause irreversible harm to the environment. Over the past few years, there has been a significant effort to use photocatalysis to remove organic dyes from contaminated water, as indicated by several source. Titanium dioxide ($TiO_2$)-based nanomaterials are the most commonly studied photocatalysts, particularly in the degradation of dyes [2-5]. $TiO_2$ is effective at breaking down pollutants under UV light without causing secondary pollution. However, its reliance on UV light makes it impractical for everyday use. Since only a small percentage of sunlight is composed of UV rays, their practical application is limited. Therefore, current research focuses on developing photocatalysts that can be activated by visible light. Based on this, significant attempts have been made to create photocatalysts with high efficiency, with a focus on copper-containing oxide photocatalysts that can effectively reduce dye contamination. This group of photocatalysts includes CuO, $Cu_2O$, $CuFe_2O_4$, $CuFeO_2$, $Cu_3Nb_2O_8$, $CuGaO_2$ and $CuBi_2O_4$ [6-12].

Copper bismuth oxide ($CuBi_2O_4$) is a type of photocatalyst that consists of copper, bismuth, and oxygen. This composite material incorporates the properties of both copper oxide (CuO) and bismuth oxide ($Bi_2O_3$). CuO is often employed as a photocatalyst for oxygen evolution and water splitting reactions. It has a broad absorption spectrum due to its wide bandgap and can efficiently capture light [13]. Nevertheless, its stability is limited, and it can be readily subjected to reduction or oxidation under certain conditions.

The compound $Bi_2O_3$ is extensively utilized as a photocatalyst for carrying out oxygen evolution reactions and splitting water. Its effectiveness in capturing light and generating free electrons is attributed

to its high electron mobility. Additionally, it can absorb a broad range of wavelengths due to its low bandgap. However, $Bi_2O_3$ is susceptible to reduction or oxidation under certain conditions and hence is not very stable. Thus, $CuBi_2O_4$ shows enhanced stability when it is mixed, as compared to its individual components CuO and $Bi_2O_3$. Its greater resistance to both reduction and oxidation enhances its durability and longevity. Additionally, it has a wider bandgap and higher electron mobility, making it better at capturing light and producing free electrons. As a result, $CuBi_2O_4$ is a more efficient photocatalyst when compared to CuO and $Bi_2O_3$ taken separately.

$CuBi_2O_4$ is a tetragonal crystal structure solid that appears yellow to orange in color when at room temperature. This material has received significant interest due to its favorable band gap range of 1.5 - 2.0 eV, which allows for a visible light response. Additionally, $CuBi_2O_4$ is known to exhibit excellent surface catalytic activities, photostability, and optical properties, further adding to its appeal as a candidate material. $CuBi_2O_4$ has been studied for its various properties that make it suitable for diverse applications such as hydrogen production, oxygen evolution, and the breakdown of organic pollutants. However, additional research is required to gain a complete understanding of its properties and its potential uses. It is also necessary to refine the techniques for its production and processing to make it more practical for real-world applications.

Various methods were employed through the wet chemical route to produce the $CuBi_2O_4$ photocatalyst, including the hydrothermal method, microwave-assisted hydrothermal synthesis, co-precipitation, sol-gel synthesis, and solid-state method [12-16]. Morphology control of the $CuBi_2O_4$ photocatalyst, such as nanocolumn arrays, nanorods, coral-shaped particles, and microspheres was studied. All results in literature indicated that the morphology of the photocatalyst played a crucial role in determining its characteristics.

Herein, we present a facile and rapid way for preparing $CuBi_2O_4$ photocatalysts by the microwave-assisted method. The reaction conditions, such as the microwave power and heating time, can be optimized to produce high-quality $CuBi_2O_4$ photocatalysts with desired properties. The microwave-assisted method has the advantage of being fast and energy-efficient, compared to traditional methods such as solid-state reaction or co-precipitation. This is because the microwaves can directly heat the photocatalyst, which reduces the need for external heating sources. The microwave-assisted method can also lead to energy savings as it requires less energy input compared to traditional methods.

In this work, a series of $CuBi_2O_4$ photocatalysts with different synthesis method including co-precipitation and microwave-assisted method were compared. The prepared phocatalysts were investigated for photocatalytic MG degradation under visible light. Based on the experimental and material characterization results, the charge transfer mechanism was proposed and discussed in detail.

## Materials and methods

### Preparation of $CuBi_2O_4$ via Co-precipitation method

All raw materials and chemical reagents used in this study are of analytical grade without further purification.

In the initial step, a mixture of 0.05 M $Bi(NO_3)_3 \cdot 5H_2O$ and 0.05 M $Cu(NO_3)_2 \cdot 3H_2O$ was prepared in a 50 mL solvent of nitric acid ($HNO_3$). Afterwards, a 2 M solution of sodium hydroxide (NaOH) was gradually added drop by drop to the mixed solution while stirring continuously, resulting in the immediate formation of a suspension solution. A brown precipitate gradually formed during continuous magnetic stirring of the obtained suspension for 10 h at room temperature. Next, the collected precipitate was washed with distilled water and ethanol, and subsequently dried in a hot air oven at 100 °C for 2 h. The $CuBi_2O_4$ product was obtained after calcining the gel at 600 °C for 3 h. The sample synthesized by co-precipitation was denoted as $CuBi_2O_4$-C.

### Preparation of $CuBi_2O_4$ via microwave-assisted method

This method involves mixing the starting materials of copper oxide and bismuth oxide in a microwave-safe container and heating them in a microwave oven. The microwave radiation causes the materials to rapidly heat up, which promotes the formation of the $CuBi_2O_4$ photocatalyst.

$CuBi_2O_4$ particles were produced through a method that involved the following steps: Initially, 0.05 M $Bi(NO_3)_3 \cdot 5H_2O$ and $Cu(NO_3)_2 \cdot 3H_2O$ solutions in $HNO_3$ solvent under constant magnetic stirring for 30 min until complete solubilization. After that, 25 mL of 2 M solution of NaOH was added to the mixture which was then autoclaved. Then, the mixture was subjected to microwave treatment at 350 watts for a duration of 10 min. Once the reaction was complete, the autoclave naturally cooled to room temperature. The product obtained was collected through centrifugation and subsequently washed with water, followed by drying in air at 100 °C for 2 h. $CuBi_2O_4$ produced using microwave-assisted technique was labeled as $CuBi_2O_4$-M.

**Material characterization**

The $CuBi_2O_4$ powders were characterized by X-ray diffraction (XRD) using a Philips X'PertMPD with Cu Ka radiation (k = 0.1546 nm). The morphologies of the samples were observed using a high-resolution field emission scanning electron microscope (FESEM, AperoS, Thermo Fisher Scientific). The Brunauer-Emmett-Teller (BET) specific surface area was measured by the $N_2$ adsorption-desorption technique on an Autosorb 1 MP, Quantachrome instrument. The optical absorption spectrum and corresponding band gap were investigated by analyzing the ultraviolet-visible diffuse reflectance spectra of the samples using the Shimadzu UV-3101PC instrument (DRS UV-Vis).

**Photocatalytic test**

Experiments were conducted to assess degradation by introducing 0.05 g samples into a 50 mL solution containing 3 ppm of MG dye in a reactor. To provide visible light irradiation, photocatalytic degradation experiments were performed using a ~54 W halogen lamp. To evaluate the ability of adsorption, the solution was stirred without light for around 30 min prior to conducting the irradiation. Additionally, an experiment was conducted on the MG dye solution without a catalyst to compare its self-degradation and photocatalytic properties. After the solution was filtered and centrifuged at every 30 min intervals, the UV-Vis spectrophotometer (Shanghai MAPADA instruments Co., Ltd) was used to measure the absorbance of the supernatant at 618 nm. The equation below defines the percentage of degradation efficiency (%D).

$$\%D = 100 \times \left(1 - \frac{C_t}{C_0}\right) \quad (1)$$

Furthermore, the rate and kinetics of MG removal can be determined by utilizing a model known as the pseudo-1$^{st}$-order equation, as presented below [17].

$$-\ln \frac{C_t}{C_0} = k_1 t \quad (2)$$

where $C_0$ is initial MG concentration and $C_t$ is remaining MG concentration at various times. $k_1$ is the pseudo 1$^{st}$-order rate constant ($min^{-1}$).

## Results and discussion

**X-ray diffraction (XRD) analysis**

The XRD patterns of $CuBi_2O_4$ samples synthesized using various techniques (co-precipitation and microwave-assisted methods) are represented in **Figure 1(a)**. The observed patterns display clear peaks at various angles, including 25.8, 27.8, 29.4, 31.0, 32.9, 34.4, 37.6, 46.1, 53.2, 55.4, 59.9 and 66.1 °. These peaks correspond to the (200), (211), (220), (002), (310), (112), (202), (411), (213), (332), (521), and (413) lattice planes of tetragonal $CuBi_2O_4$ (JCPDF 42-0334), respectively. Notably, there were no other secondary phases detected in the diffraction peaks. This suggests that both samples exhibited crystallization in a pure tetragonal phase.

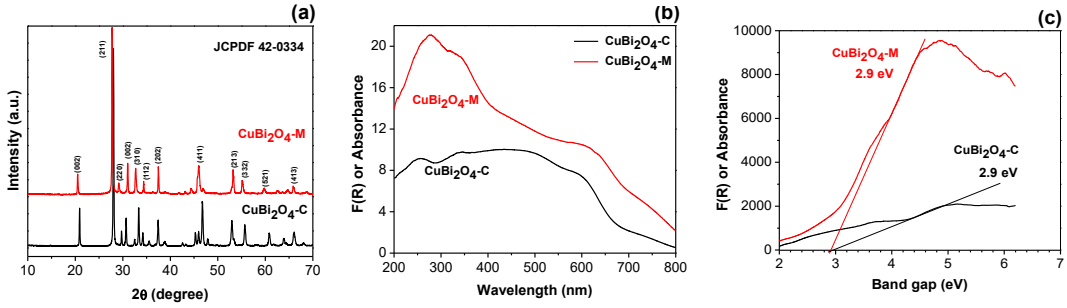


**Figure 1** (a) X-ray diffraction patterns of prepared $CuBi_2O_4$ at different synthesis method, (b) UV-Vis diffuse reflectance spectra, and (c) Tauc plot for band gap analysis.

To compare this work with the literature reports, synthesis of $CuBi_2O_4$ by various experimental methods is presented in **Table 1**. It is to be noted that microwave-assisted and co-precipitation methods in this work are compared with different wet chemical routes, as stated in the introduction section [12-16],

Despite employing the same synthesis method, variations in experimental conditions led to differences in the crystal structure and morphology of $CuBi_2O_4$ photocatalysts.

**Table 1** Comparison the effect of the synthesis methods of $CuBi_2O_4$ on its morphology, crystal structure and photocatalytic activity.

| Synthesis method | Morphology | Crystal structure | Applications | Ref. |
|---|---|---|---|---|
| Hydrothermal | Nanocolumn Arrays and Nanorods | Tetragonal phase | - Photodegradation of methylene blue (MB) under visible light for 0.5 h.<br>- Photodegradation efficiency = 91 %. | [12] |
| Microwave-assisted hydrothermal synthesis | Coral-shaped particles and Spheres composed of nanorods | Tetragonal phase | - Photoreduction process from $CO_2$ to $CH_4$.<br>- Conversion efficiency = 90 %. | [13] |
| Co-precipitation | Irregular microspheres | Tetragonal phase | Supercapacitor electrode material | [14] |
| Sol-gel | Agglomerated morphologies | Monoclinic phase | - Photodegradation of methylene blue (MB) under visible light for 1 h.<br>- Photodegradation efficiency = 90 %. | [15] |
| Solid-state | N/A | Tetragonal phase | - Decomposition of acetaldehyde to $CO_2$ under LED light for 2.5 - 3 h. | [16] |
| Microwave-assisted | Flower-like microspheres | Tetragonal phase | - Photodegradation of malachite green under visible light for 2 h.<br>- Photodegradation efficiency = 83.4 %. | This study |
| Co-precipitation | Spherical aggregation | Tetragonal phase | - Photodegradation of malachite green under visible light for 2 h.<br>- Photodegradation efficiency = 52.3 % | This study |

It is established that subjecting materials to heat treatment can lead to an increase in grain size, a phenomenon that is evident in the full width at half maximum (FWHM, β) of the XRD peak. Utilizing these FWHM values, the crystallite size was determined through the Scherrer equation, which is expressed as follows:

$$D = \frac{k \times \lambda}{\beta \times \mathrm{Cos}\theta} \quad (3)$$

where D is the crystallite size, K is the numerical value known as the crystallite shape factor, conventionally set at 0.9, λ is the wavelength of X-rays used (usually 1.5406 Å for Cu $K_\alpha$) and θ is the diffraction angle (2θ = 27.8 ° corresponding to (211) plane). The average crystallite size is obtained as 50.5 nm for the $CuBi_2O_4$-M, while the crystallite size for the 600 °C heat-treated $CuBi_2O_4$-C sample is got to be 65.8 nm. The specific surface area of $CuBi_2O_4$-C is expected to be reduced in comparison to $CuBi_2O_4$-M due to the formation of larger grains or aggregates resulting from the high-temperature calcination process.

**UV-Vis diffuse reflectance spectra and band gap analysis**

UV-Vis diffuse reflectance spectra of $CuBi_2O_4$ with different synthesis method were investigated and displayed in **Figures 1(b) - 1(c)**. The $CuBi_2O_4$-C and $CuBi_2O_4$-M showed good visible light absorption, as shown in **Figure 1(b)**. Tauc plots were applied to determine the band energy of different $CuBi_2O_4$ samples, as illustrated in **Figure 1(c)**. The slope of the tangent indicates that there is not a noticeable variation in the band gap (approximately 2.9 eV) between the $CuBi_2O_4$ samples that were synthesized using different methods. Therefore, the photocatalytic degradation rate of $CuBi_2O_4$ in this study should not be attributed to the optical properties.

**Field scanning electron microscope (FESEM)**

The FESEM micrographs of $CuBi_2O_4$ displayed in **Figure 2** reveal that the morphologies are significantly influenced by the synthesis routes. **Figures 2(a) - 2(b)** demonstrate that co-precipitation produces $CuBi_2O_4$ particles ($CuBi_2O_4$-C) with a spherical shape and rough surface, measuring between 1.0 - 3.0 μm in diameter. In addition, high-temperature calcination can cause spherical samples to fuse or agglomerate together. The $CuBi_2O_4$-M (**Figures 2(c) - 2(d)**) synthesized by microwave-assisted method mainly presents a uniform flower-like microspheres with a diameter of 1.0 - 3.0 μm, which assembled by cube-like subunits. Flower-like microspheres with a well-defined structure can provide an effective platform for photocatalysis, due to their high surface area and efficient adsorption properties, which agreed well with BET surface area presented in **Table 2**.

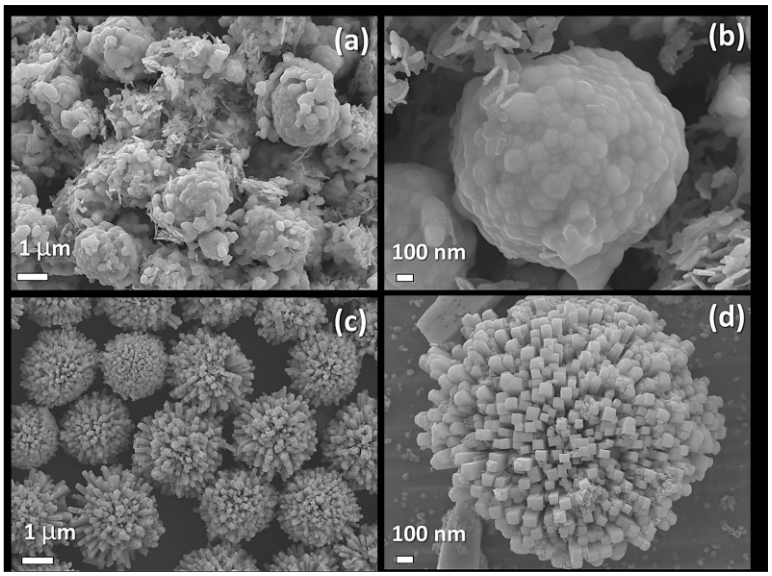


**Figure 2** SEM images of $CuBi_2O_4$ prepared with (a), (b) co-precipitation and (c), (d) Microwave-assisted methods.

**Brunauer-Emmett-Teller (BET)**

According to the data presented in **Table 2**, the $CuBi_2O_4$-M sample exhibited higher BET surface areas and pore volumes compared to the $CuBi_2O_4$ sample. The greater surface area and pore volume observed in $CuBi_2O_4$-M compared to $CuBi_2O_4$-C can be attributed to the unique morphology (flower-like microspheres) and structural characteristics introduced by the specific modification process that results in a more porous and textured surface. This increased porosity can enhance the accessibility of active sites and facilitate better adsorption and catalytic properties, which contribute to the higher surface area and pore volume of $CuBi_2O_4$-M when compared to $CuBi_2O_4$-C. This result can be correlated in line with the crystallite size obtained through XRD analysis. The average crystallite size for the as-prepared and 600 °C heat-treated sample ($CuBi_2O_4$-C) and $CuBi_2O_4$-M are 65.8 and 50.5 nm, respectively. It is evident that increased size would lead to a decrease in the specific surface area.

**Table 2** Surface properties of $CuBi_2O_4$-C and $CuBi_2O_4$-M samples.

| Sample | Surface area ($m^2/g$) | Pore volume ($cm^3/g$) | Pore size (nm) |
|---|---|---|---|
| $CuBi_2O_4$-C | 4.3272 | 0.0060 | 13.5816 |
| $CuBi_2O_4$-M | 10.6207 | 0.0236 | 12.2368 |

**Photocatalytic degradation of malachite green dye**

The photocatalytic degradation for MG over the $CuBi_2O_4$-M was evaluated and compared with the $CuBi_2O_4$-C in **Figure 3(a)**. At the start of the adsorption experiment, the flower-like $CuBi_2O_4$-M microsphere, synthesized via microwave-assisted method, showed rapid adsorption of around 51.3 % of MG dye molecules on their surface due to their high specific surface area. Meanwhile $CuBi_2O_4$-C showed an adsorption efficiency of 28.9 %, which tended to saturate after 30 min. $CuBi_2O_4$-M exhibited the highest photocatalytic activity among the 2 samples, with an approximate degradation rate of 83.4 % after 120 min of visible light irradiation, while the co-precipitated $CuBi_2O_4$-C sample had a degradation rate of 52.3 %. Moreover, the test demonstrated that the decolorization of MG dye solution was approximately 17.3 % in the absence of a photocatalyst. According to the kinetics results in **Figure 3(b)**, it demonstrates that $CuBi_2O_4$-M had the highest degradation efficiency (0.0144 $min^{-1}$), with a rate constant 2 times higher than that of $CuBi_2O_4$-C (0.0071 $min^{-1}$). To compare this work with the literature reports, performance of $CuBi_2O_4$ by various synthesis methods with different morphologies is also presented in **Table 1**. Among all the cases, the $CuBi_2O_4$ photocatalyst prepared in nanocolumn arrays and nanorods prepared by hydrothermal showed much better degradation efficiency of 91 % in 0.5 h under visible light irradiation [12]. Regarding the $CuBi_2O_4$ synthesized using the microwave-assisted technique in this work, while its

performance in degrading MG is not the best (83.4 % degradation), it demonstrates a remarkable advantage in terms of rapid material preparation, taking only 10 min using a conventional household microwave.

**Figure 4** shows a proposed process for the degradation of MG via $CuBi_2O_4$ photocatalysts. When exposed to visible light, electron (e−) transfer from the valence band (VB) to the conduction band (VB) creates photoinduced holes (h+) in the VB. Oxygen ($O_2$) captures electrons (e−) and generates super oxide radical anion ($O_2$ •$^-$), which have the capability to effectively decompose MG. On the other hand, the positive charges ($h^+$) in the VB can directly convert MG into its degradation products.

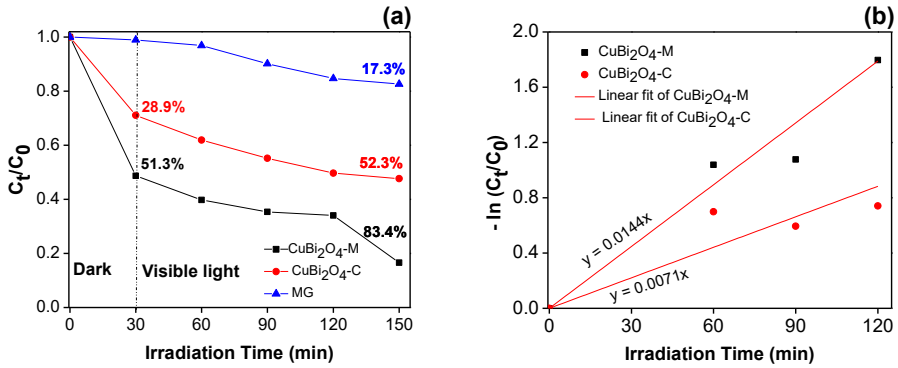


**Figure 3** (a) $C_t/C_0$ and (b) kinetic plot.

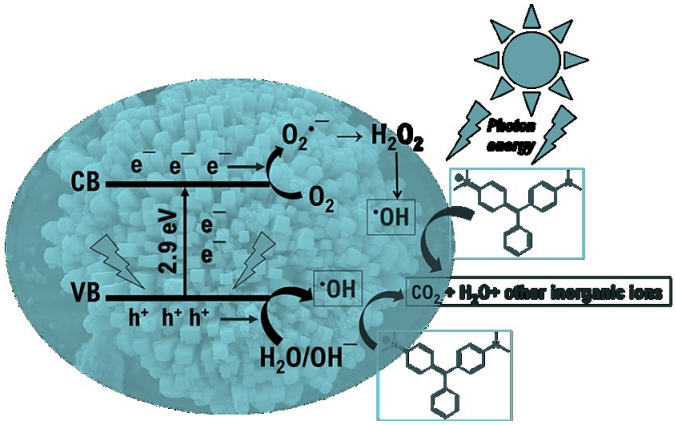


**Figure 4** Proposed photocatalytic mechanism for $CuBi_2O_4$.

## Conclusions

In this study, the $CuBi_2O_4$ powders prepared with microwave-assisted synthesis and co-precipitation had the tetragonal phase. Of the 2 methods, microwave-assisted synthesis demonstrated to be the superior option for producing $CuBi_2O_4$ with a microsphere structure, owing to its shorter reaction time and easier operation as compared to co-precipitation synthesis. The photocatalytic activity of $CuBi_2O_4$-M was higher than that of $CuBi_2O_4$-C due to its flower-shaped microsphere because of its large surface area and unique structure, which allow for enhanced light absorption and improved photocatalytic performance. Therefore, this research suggests an alternate approach, which is a fast and efficient technique for the production of $CuBi_2O_4$ photocatalyst with a complex microsphere structure. Additionally, the complex microsphere structure offers a high degree of porosity, which facilitates the movement of electrons, thereby increasing the efficiency of photocatalytic reactions. The unique structure of the microsphere offers greater light scattering and reflection, leading to increased absorption of light and greater utilization of the energy in the photocatalytic process. As a result, $CuBi_2O_4$ with a complicated microsphere structure is preferred over other materials for photocatalytic applications. Utilizing $CuBi_2O_4$ for the removal of emerging contaminants, heavy metals, and organic pollutants from water sources can contribute to solving pressing environmental challenges.

**Acknowledgements**

The authors gratefully to the Department of Chemistry, Faculty of Science, Naresuan University, Thailand for the financial support (grant no. R2566E087).

**References**

[1] PO Oladoye, TO Ajiboye, WC Wanyonyi, EO Omotola and ME Oladipo. Insights into remediation technology for malachite green wastewater treatment. *Water Sci. Eng.* 2023; **6**, 261.

[2] X Chen and A Selloni. Introduction: Titanium dioxide ($TiO_2$) nanomaterials. *Chem. Rev.* 2014; **114**, 9281.

[3] FD Angelis, CD Valentin, S Fantacci, A Vittadini and A Selloni. Theoretical studies on anatase and less common $TiO_2$ phases: Bulk, surfaces, and nanomaterials. *Chem. Rev.* 2014; **19**, 9708.

[4] VH Bui, TK Vu, HT To and N Negishi. Application of $TiO_2$-ceramic/UVA photocatalyst for the photodegradation of sulfamethoxazole. *Sustain. Chem. Pharm.* 2022; **26**, 100617.

[5] C Xia, TH Chuong Nguyen, XC Nguyen, SY Kim, D Le Tri Nguyen, P Raizada, P Singh, V Nguyen, CC Nguyen, VC Hoang and QV Le. Emerging cocatalysts in $TiO_2$-based photocatalysts for light-driven catalytic hydrogen evolution: Progress and perspectives. *Fuel* 2022; **307**, 121745.

[6] P Raizada, A Sudhaik, S Patial, V Hasija, AA Parwaz Khan, P Singh, S Gautam, M Kaur and V Nguyen. Engineering nanostructures of CuO-based photocatalysts for water treatment: Current progress and future challenges. *Arabian J. Chem.* 2020; **13**, 8424.

[7] MW Zheng, SJ Yang, YC Pu and SH Liu. Mechanisms of biochar enhanced $Cu_2O$ photocatalysts in the visible-light photodegradation of sulfamethoxazole. *Chemosphere* 2022; **307**, 135984.

[8] M Zangiabadi, A Saljooqi, T Shamspur and A Mostafavi. Evaluation of GO nanosheets decorated by $CuFe_2O_4$ and CdS nanoparticles as photocatalyst for the degradation of dinoseb and imidacloprid pesticides. *Ceram. Int.* 2020; **46**, 6124.

[9] F Darkhosh, M Lashanizadegan, AR Mahjoub and AHC Khavar. One pot synthesis of $CuFeO_2$@ expanding perlite as a novel efficient floating catalyst for rapid degradation of methylene blue under visible light illumination. *Solid State Sci.* 2019; **91**, 61.

[10] S Kamimura, N Murakami, T Tsubota and T Ohno. Fabrication and characterization of a p-type $Cu_3Nb_2O_8$ photocathode toward photoelectrochemical reduction of carbon dioxide. *Appl. Catal. B Environ.* 2015; **174-175**, 471.

[11] M Choi, S Yagi, Y Ohta, K Kido and T Hayakawa. Estimation of delafossite p-type $CuGaO_2$/ZnO hybrids as semiconductor photocatalyst by controlling particle size. *J. Phys. Chem. Solid.* 2021; **150**, 109845.

[12] Y Wang, F Cai, P Guo, Y Lei, Q Xi and F Wang. Short-time hydrothermal synthesis of $CuBi_2O_4$ nanocolumn arrays for efficient visible-light photocatalysis. *Nanomaterials* 2019; **9**, 1257.

[13] LS Ribeiro, IM Pinatti, JA Torres, AS Giroto, F Lesse, E Longo, C Ribeiro and AE Nogueira. Rapid microwave-assisted hydrothermal synthesis of $CuBi_2O_4$ and its application for the artificial photosynthesis. *Mater. Lett.* 2020; **275**, 128165.

[14] YC Zhang, H Yang, WP Wang, HM Zhang, RS Li, XX Wang and RC Yu. A promising supercapacitor electrode material of $CuBi_2O_4$ hierarchical microspheres synthesized via a coprecipitation route. *J. Alloy. Comp.* 2016; **684**, 707.

[15] J Zhang and Y Jiang. Preparation, characterization and visible photocatalytic activity of $CuBi_2O_4$ photocatalyst by a novel sol-gel method. *J. Mater. Sci. Mater. Electron.* 2015; **26**, 4308.

[16] M Nishikawa, S Yuto, T Hasegawa, W Shiroishi, H Honghao, Y Nakabayashi, Y Nosaka and N Saito. Compositing effects of $CuBi_2O_4$ on visible-light responsive photocatalysts. *Mater. Sci. Semicond. Process.* 2017; **57**, 12.

[17] A Balakrishnan, K Gopalram and S Appunni. Photocatalytic degradation of 2,4-dicholorophenoxyacetic acid by $TiO_2$P modified catalyst: Kinetics and operating cost analysis. *Environ. Sci. Pollut. Res.* 2021; **28**, 33331.